Appl. Phys. B 84, 617–625 (2006)
DOI: 10.1007/s00340-006-2377-9

Applied Physics B
Lasers and Optics

A. MIFFRE[1,2]
M. JACQUEY[1]
M. BÜCHNER[1]
G. TRÉNEC[1]
J. VIGUÉ[1,✉]

Vibration-induced phase noise in Mach–Zehnder atom interferometers

[1] Laboratoire Collisions Agrégats Réactivité – IRSAMC, Université Paul Sabatier and CNRS UMR 5589, 118, Route de Narbonne, 31062 Toulouse Cedex, France
[2] Université de Provence and CNRS UMR 6633, Centre de saint Jérôme case C21, 13397 Marseille Cedex 20, France

Received: 4 April 2006/Revised version: 15 June 2006
Published online: 27 July 2006 •

ABSTRACT The high inertial sensitivity of atom interferometers has been used to build accelerometers and gyrometers, but this property makes these interferometers very sensitive to the laboratory seismic noise. This seismic noise induces a phase noise which is large enough to reduce the fringe visibility in many cases. We develop here a model calculation of this phase noise applicable to a wide class of Mach–Zehnder atom interferometers and we apply this model to our thermal lithium interferometer. We are thus able to explain the observed dependence of the fringe visibility on the diffraction order. The dynamical model developed in the present paper should be very useful to further reduce this phase noise in atom interferometers and this reduction should open the way to improved interferometers.

PACS 03.75.Dg; 39.20.+q; 42.50.Vk

1 Introduction

Atom interferometers have a large inertial sensitivity [1, 2], which has been used to develop sensitive accelerometers [3–10] and gyrometers [11–16]. However, because of this large sensitivity, a high mechanical stability of the experiment is required. This problem was recognized in 1991 by Pritchard and co-workers [17], who were obliged to actively control the vibrations of the diffraction gratings of their Mach–Zehnder thermal atom interferometer. Since this work, various types of vibration control were developed: as an example, a very efficient control was developed by Chu and coworkers [6, 7] for the measurement of the local acceleration of gravity g. The problem obviously depends on the interferometer design and the present paper is devoted to an analysis of the vibration problem in three-grating Mach–Zehnder interferometers operated with thermal atoms. In 2005, the group of Arndt and Zeilinger made an experimental study of the effect of vibrations on the signals of their Talbot–Lau interferometer operated with fullerenes [18].

In the present paper, we are going to evaluate the phase noise induced by mechanical vibrations in a Mach–Zehnder thermal atom interferometer. In such an interferometer, the three gratings used to diffract the atomic wave are usually supported by a rail and we have developed a model of the dynamics of this rail, using elasticity theory. Thanks to some reasonable assumptions, this model is simple but it remains very general. With this model, we analyze how the vibrations displace and distort the rail. We can thus understand how the various frequency components of the seismic noise contribute to the interferometer phase noise. We then apply this calculation to the case of our interferometer: we use a very stiff rail and this arrangement has strongly reduced the effect of vibrations with respect to previous interferometers. In our apparatus, the vibration-induced rotations of the rail provide the dominant contribution to the phase noise. Using the measured values of the seismic noise in our setup, we have evaluated the phase noise, with a result in reasonable agreement with the value deduced from fringe-visibility measurements.

The paper is organized in the following way: Sect. 2 recalls classical results concerning the inertial sensitivity of three-grating Mach–Zehnder interferometers. Section 3 describes theoretically the motion and deformation of the rail holding the gratings and the resulting phase effect. Section 4 describes the rail of our interferometer and applies the present theory to this case. Section 5 discusses how to further reduce the vibration-induced phase noise in this type of atom interferometer.

2 Sensitivity of Mach–Zehnder atom interferometers to accelerations and rotations

Atom interferometers are very sensitive to inertial effects [1, 2]. We consider a three-grating Mach–Zehnder atom interferometer represented schematically in Fig. 1 and we follow a tutorial argument presented by Schmiedmayer et al. in [19]. Each atomic beam is represented by a plane wave. When a plane wave $\Psi = \exp[\mathrm{i}\boldsymbol{k}\boldsymbol{r}]$ is diffracted by a grating G_j, diffraction of order p produces a plane wave:

$$\Psi_{\mathrm{d}}(\boldsymbol{r}) = \alpha_j(p)\exp\left[\mathrm{i}\boldsymbol{k}\cdot\boldsymbol{r} + \mathrm{i}\,p\boldsymbol{k}_{\mathrm{G}j}\cdot(\boldsymbol{r}-\boldsymbol{r}_j)\right] . \quad (1)$$

Here $\alpha_j(p)$ is the diffraction amplitude; $\boldsymbol{k}_{\mathrm{G}j}$ is the grating wave vector, in the grating plane and perpendicular to its lines, with a modulus $k_{\mathrm{G}} = 2\pi/a$, the same for the three gratings. The grating period a is equal to $a = \lambda_{\mathrm{L}}/2$ in the case of diffraction by a laser standing wave with a laser wavelength λ_{L}. This

✉ Fax: +33 561558317, E-mail: jacques.vigue@irsamc.ups-tlse.fr

equation is exact for Bragg diffraction and a good approximation if $\boldsymbol{k}$ and $\boldsymbol{k}_{\mathrm{G}j}$ are almost perpendicular and $|\boldsymbol{k}_{\mathrm{G}j}| \ll |\boldsymbol{k}|$. Finally, $\boldsymbol{r}_j$ is a coordinate which measures the position of a reference point in grating G_j. Because of the presence of $\boldsymbol{r}_j$ in (1), the phase of the diffracted wave depends on the position of the grating in its plane and this dependence explains the inertial sensitivity of atom interferometers.

The waves exiting from the interferometer by exit 1 (see Fig. 1) are Ψ_{u} following the upper path (diffraction orders p, $-p$ and 0) and Ψ_{l} following the lower path (diffraction orders 0, p and $-p$). These two waves produce an intensity proportional to $|\Psi_{\mathrm{u}} + \Psi_{\mathrm{l}}|^2$, which must be integrated over the detector surface. The condition $\boldsymbol{k}_{\mathrm{G1}} + \boldsymbol{k}_{\mathrm{G3}} = 2\boldsymbol{k}_{\mathrm{G2}}$ must be fulfilled to maximize the fringe visibility. We will assume that this condition is realized and that the grating wave vectors $\boldsymbol{k}_{\mathrm{G}j}$ are parallel to the x axis. Then, the interferometer output signal I measured at exit 1 is given by

$$I = I_{\mathrm{m}}\left[1 + \mathcal{V}\cos\Phi_{\mathrm{p}}\right] \text{ with } \Phi_{\mathrm{p}} = pk_{\mathrm{G}}\left[2x_2 - x_1 - x_3\right] , \quad (2)$$

where I_{m} is the mean intensity and $\mathcal{V}$ is the fringe visibility defined by $\mathcal{V} = (I_{\max} - I_{\min})/(I_{\max} + I_{\min})$. When the gratings are moving, we must correct the grating-position-dependent phase Φ_{p} in (2) by considering for each atomic wave packet the position of the grating G_j at the time t_j when the wave packet goes through this grating:

$$\Phi_{\mathrm{p}} = pk_{\mathrm{G}}\left[2x_2(t_2) - x_1(t_1) - x_3(t_3)\right] . \quad (3)$$

If $T = L_{12}/v$ is the atom's time of flight from one grating to the next (with $L_{12} = L_{23}$ and v being the atom's velocity), t_j are given by $t_1 = t - T$ and $t_3 = t + T$, where t_2 has been denoted t. We expand Φ_{p} in powers of T by introducing the x components of the velocity $v_{jx}(t)$ and acceleration $a_{jx}(t)$ of grating G_j measured with reference to a Galilean frame. We assume that the accelerations can be considered as constant during the total time of flight $2T$. The phase Φ_{p} becomes

$$\Phi_{\mathrm{p}} = \Phi_{\mathrm{bending}} + \Phi_{\mathrm{Sagnac}} + \Phi_{\mathrm{acc.}} , \quad (4)$$

with $\Phi_{\mathrm{bending}} = pk_{\mathrm{G}}\delta(t)$, where the bending $\delta(t) = 2x_2(t) - x_1(t) - x_3(t)$ is so called because it vanishes when the three gratings are aligned. The second term $\Phi_{\mathrm{Sagnac}} = pk_{\mathrm{G}}(v_{3x}(t) - v_{1x}(t))T$ represents the Sagnac effect because the velocity difference can be written $v_{3x}(t) - v_{1x}(t) = 2\Omega_y L_{12}$, where Ω_y is the y component of the angular velocity of the interferometer rail. Finally, the third term $\Phi_{\mathrm{acc.}} = pk_{\mathrm{G}}(a_{1x}(t) + a_{3x}(t))T^2/2$ describes the sensitivity to linear acceleration [1], slightly modified because the accelerations of the gratings G_1 and G_3 are different. One should average over the velocity distribution of the incident atomic beam but, if this velocity distribution is not too broad as in supersonic beams, it is an excellent approximation to use for T the value corresponding to the mean velocity u.

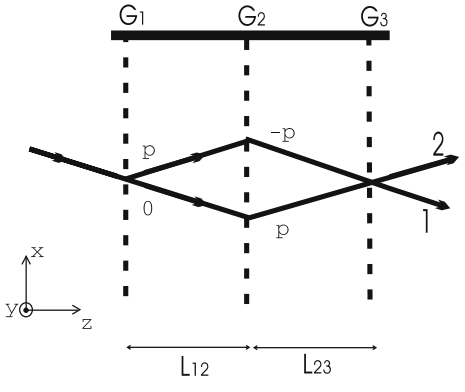

FIGURE 1 Schematic drawing of a three-grating Mach–Zehnder atom interferometer, in the Bragg diffraction geometry. A collimated atomic beam is successively diffracted by three gratings G_1, G_2 and G_3. The diffraction orders are indicated on the various paths. Two exit beams, labelled 1 and 2, carry complementary signals. The x, y and z axes are defined

3 Theoretical analysis of the rail dynamics

To calculate the phase Φ_{p}, we are going to relate the positions $x_j(t_j)$ of the three gratings to the mechanical properties of the rail holding them and to its coupling to the environment. A one-dimensional theory of the rail is sufficient to describe the grating motions in the x direction. As we want to know the $x_j(t_j)$ functions typically up to 10^3 Hz, the rail must be treated as an elastic object.

3.1 *Equations of motion of the rail deduced from elasticity theory*

The rail will be described as an elastic object of length $2L$, along the z direction, which can bend only in the x direction. The rail is made of a material of density ϱ and Young's modulus E. The cross section, with a shape independent of the z coordinate, is characterized by its area $A = \int \mathrm{d}x\,\mathrm{d}y$ and by the moment $I_y = \int x^2\,\mathrm{d}x\,\mathrm{d}y$, the x origin being taken on the neutral line. The neutral line is described by a function $X(z, t)$ which measures the position of this line with respect to a Galilean frame linked to the laboratory (in this paper, we forget that, because of Earth rotation, the laboratory is not a Galilean frame). Elasticity theory [20] gives a relation between the t and z derivatives of X:

$$\varrho A\frac{\partial^2 X}{\partial t^2} = -EI_y\frac{\partial^4 X}{\partial z^4} . \quad (5)$$

The rail is subjected to forces and torques exerted by its supports located at its two ends at $z = \varepsilon L$, where $\varepsilon = \pm$ labels the rail ends. The forces and torques are given by

$$F_{x\varepsilon} = -\varepsilon EI_y\frac{\partial^3 X}{\partial z^3}\,(z = \varepsilon L) , \quad (6)$$

$$M_{y\varepsilon} = \varepsilon EI_y\frac{\partial^2 X}{\partial z^2}\,(z = \varepsilon L) . \quad (7)$$

These torques and forces depend on the suspension of the rail. We assume that the torques vanish: this assumption seems to be good as this property would be verified if the suspension was made in one point at each end of the rail. We consider that the forces are the sum of an elastic term proportional to the relative displacement and a damping term proportional to the relative velocity:

$$F_{x\varepsilon} = -K_\varepsilon[X(\varepsilon L, t) - x_\varepsilon(t)] - \mu_\varepsilon\frac{\partial[X(\varepsilon L, t) - x_\varepsilon(t)]}{\partial t} . \quad (8)$$

Here $x_\varepsilon(t)$ is the coordinate of the support at $z = \varepsilon L$. The spring constants K_ε and the damping coefficients μ_ε may not be the same at the two ends of the rail. We have chosen to describe all the damping effects by introducing only damping terms in $F_{x\varepsilon}$. This is an approximation as other sources of damping exist and the damping terms have an effective character, which means that a detailed comparison with experiment may require us to use frequency-dependent μ_ε values.

3.2 *Solutions of these equations*

We introduce the Fourier transforms $X(z, \omega)$ and $x_\varepsilon(\omega)$ of the functions $X(z, t)$ and $x_\varepsilon(t)$. The general solution of (5) is

$$X(z, \omega) = a \sin(\kappa z) + b \cos(\kappa z) + c \sinh(\kappa z) + d \cosh(\kappa z) , \tag{9}$$

where a, b, c and d are the four ω-dependent amplitudes of the spatial components of the function $X(z, \omega)$. ω and κ are related by

$$\varrho A \omega^2 = E I_y \kappa^4 . \tag{10}$$

Equations (6)–(8) relate a, b, c and d to the source terms $x_\varepsilon(\omega)$. Thanks to the assumption $M_{y\varepsilon} = 0$, c and d are related to a and b:

$$\begin{aligned} c &= a \sin(\kappa L)/ \sinh(\kappa L) , \\ d &= b \cos(\kappa L)/ \cosh(\kappa L) , \end{aligned} \tag{11}$$

and we obtain two equations relating a and b to $x_\varepsilon(\omega)$:

$$\alpha_\varepsilon a + \varepsilon \beta_\varepsilon b = \varepsilon \gamma_\varepsilon x_\varepsilon(\omega) , \tag{12}$$

where α_ε, β_ε and γ_ε are given in the appendix. If we know the functions $x_\varepsilon(\omega)$, we can calculate the a, b, c and d amplitudes and the motion of any point of the rail as a function of time.

3.3 *Analysis of the various regimes*

To simplify the analysis in the present paragraph, we assume that $K_- = K_+ = K$ and $\mu_- = \mu_+ = 0$. The first assumption decouples the two pendular motions described below and the second assumption makes the resonance infinitely sharp. In the appendix, we write the equations in the general case and we calculate the Q-factors of the resonances.

When ω increases, the present theory describes the transition from a low-frequency dynamics in which the rail moves almost like a solid to a high-frequency dynamics with a series of bending resonances. When the frequency is low enough, $\kappa L \ll 1$ because $\kappa \propto \sqrt{\omega}$ is also small and we may expand the functions of κL up to third order (cubic terms in κL are needed to transmit a transverse force through the rail) and two resonances appear corresponding to pendular oscillations of the rail. The first resonance appears on the b amplitude, when R given by (A.2) verifies $R \approx 1$. This resonance corresponds to an in-phase oscillation of the two ends of the rail, with a frequency $\omega_{\rm osc} = \sqrt{K/(\varrho A L)}$. The second resonance, which appears on the a amplitude when $R \approx 3$, describes a rotational oscillation of the rail around its center with a frequency $\omega_{\rm rot} = \omega_{\rm osc}\sqrt{3}$. If the two spring constants K_ε are different, these two resonances are mixed (each resonance appears on the a and b amplitudes) and their frequency difference increases.

For larger frequencies, κL becomes too large to use expansions of the functions in powers of κL. We then enter the range of bending resonances of the rail. If the forces $F_{x\varepsilon}$ are weak enough, these resonances are almost those of the isolated rail, which are obtained by writing that the equation system (12) has a nonvanishing solution when the applied forces vanish and the resonance condition is

$$\cos(2\kappa L) \cosh(2\kappa L) = 1 , \tag{13}$$

which defines a series of κ_n values given approximately by

$$\kappa_n L \approx (2n+3)\frac{\pi}{4} + \frac{(-1)^n}{\cosh\left[(2n+3)\pi/2\right]} . \tag{14}$$

n starts from 0 (a more accurate value of $\kappa_0 L$ is $\kappa_0 L = 2.365$) and $a = c = 0$ when n is even while $b = d = 0$ when n is odd. ω_n is deduced from κ_n, using (10). For a given length L, the wave vectors κ_n are fixed, but the resonance frequencies ω_n increase with the stiffness of the rail measured by the quantity $EI_y/(\varrho A)$. Finally, all the resonance frequencies ω_n are related to ω_0 by $\omega_n = \omega_0(\kappa_n/\kappa_0)^2$, with

$$\omega_0 = 5.593\sqrt{EI_y/(\varrho A L^4)} . \tag{15}$$

Introducing the period T_0 of the first bending resonance, $T_0 = 2\pi/\omega_0$, we may rewrite (10) in the form $(\kappa L)^2 = 0.890 \times \omega T_0$.

3.4 *Effect of vibrations on the interferometer signal*

The Fourier component $\Phi_{\rm p}(\omega)$ of the phase $\Phi_{\rm p}$ given by (3) can be expressed as a function of the amplitudes $a(\omega)$ and $b(\omega)$ given by solving the system of equations (12). We assume that the gratings are on the neutral line, which means that $x_i(t_i) = X(z_i, t_i)$, with $z_1 = -L_{12}$ and $t_1 = t - T$ for grating G_1, $z_2 = 0$ and $t_2 = t$ for grating G_2 and $z_3 = +L_{12}$ and $t_3 = t + T$ for grating G_3. We obtain

$$\begin{aligned} &\frac{\Phi_{\rm p}(\omega)}{2pk_{\rm G}} \\ &= \Bigg[b(\omega) \left(1 - \cos(\kappa L_{12}) + (1 - \cosh(\kappa L_{12})) \frac{\cos(\kappa L)}{\cosh(\kappa L)} \right) \\ &+ {\rm i} a(\omega) \left(\sin(\kappa L_{12}) + \sinh(\kappa L_{12}) \frac{\sin(\kappa L)}{\sinh(\kappa L)} \right) \sin(\omega T) \\ &+ b(\omega) \left(\cos(\kappa L_{12}) + \cosh(\kappa L_{12}) \frac{\cos(\kappa L)}{\cosh(\kappa L)} \right) \\ &\times (1 - \cos(\omega T)) \Bigg] \end{aligned} \tag{16}$$

where the different lines correspond to the bending, the Sagnac and the acceleration terms in this order. We can simplify this equation by making an expansion in powers of ωT

up to power 2 and in powers of κL or κL_{12} up to fourth order:

$$\frac{\Phi_{\mathrm{p}}(\omega)}{pk_{\mathrm{G}}} \approx b\left(\frac{6(\kappa L)^2(\kappa L_{12})^2-(\kappa L_{12})^4}{6}\right) + 4\mathrm{i}a\kappa L_{12}\left(1-\frac{(\kappa L)^2}{6}\right)\omega T \times 2b(\omega T)^2 . \quad (17)$$

As in (4), we recognize the instantaneous bending of the rail (first line, independent of the time of flight T), the Sagnac term (second line, linear in T) and the acceleration term (third line, proportional to T^2). With the same approximations, a and b are given by (A.4) and (A.5). To further simplify the algebra, we replace the distance L_{12} by L (L_{12} will usually be close to L), and we obtain

$$\frac{\Phi_{\mathrm{p}}(\omega)}{pk_{\mathrm{G}}} \approx [x_+(\omega)-x_-(\omega)]\,\frac{3\mathrm{i}\omega T}{3-R} + [x_+(\omega)+x_-(\omega)]\,\frac{0.330(\omega T_0)^2+(\omega T)^2}{2(1-R)} , \quad (18)$$

where R is given by (A.2).

These three equations (16), (17) and (18) are the main theoretical results of the present paper. Equation (18) has a limited validity, because of numerous approximations, but it gives a very clear view of the various contributions. The first term, proportional to $[x_+(\omega)-x_-(\omega)]$ and to the time of flight T, describes the effect of the rotation of the rail excited by the out-of-phase motion of its two ends. This term, which is independent of the stiffness of the rail, is sensitive to the rail suspension through the $3-R$ denominator, which is very small when $\omega \approx \omega_{\mathrm{rot}}$. The second term is the sum of the bending term, in $(\omega T_0)^2$, and the acceleration term, in $(\omega T)^2$. Both are terms in ω^2 and they also have the same sensitivity to the suspension of the rail, through the $1-R$ denominator, which is very small when $\omega \approx \omega_{\mathrm{osc}}$. Furthermore, the bending term is very small if the rail is very stiff, i.e. if the T_0 value is very small.

For larger frequencies ($\omega T \gtrsim 1$ or $\kappa L \gtrsim 1$), we must use (16). We may note that, because $\omega \gg \omega_{\mathrm{osc}}, \omega_{\mathrm{rot}}$, the a and b amplitudes will be small except near the bending resonances, which appear on one or the other of these two amplitudes and do not contribute to the same terms of $\Phi_{\mathrm{p}}(\omega)$.

4 Application of the present analysis to our interferometer

In this section, we are going to describe the rail of our interferometer and to characterize its vibrations.

4.1 *Information coming from previous experiments*

When we built our interferometer in 1998, we knew that the vibration amplitudes encountered by Pritchard [17, 19] and Siu Au Lee [24, 25] in their interferometers were large: for instance, we read in [17] that $\sqrt{\langle\delta(t)^2\rangle}$ is close to 500 nm after passive isolation by rubber pads. In this experiment, each grating was supported on a flange of the vacuum pipe, which played the role of the rail. In the interferometer of Siu Au Lee and co-workers, a rail inspired by the three-rod design used for laser cavities was built [25] but, with a rod diameter close to 15 mm, the rail was not very stiff. In both experiments, servo loops were used to reduce $\delta(t)$ and this reduction was necessary to observe interference signals.

4.2 *The rail of our interferometer*

Rather than using servo loops, we decided to achieve the best possible grating stability by building a very stiff rail. We had to choose the material of the rail, its shape and its suspension, the main constraint being that the rail had to fit inside the DN250 vacuum pipe of our atom interferometer. The material must have a large value of E/ϱ ratio (Young's modulus divided by density): we have chosen aluminium alloy rather than steel, both metals having almost the same E/ϱ ratio, because aluminium alloy is lighter and easier to machine. The shape of the rail must give the largest ratio I_y/A with an open structure for vacuum requirements: we choose to make the rail as large as possible in the x direction and rather thick to insure a good stiffness in the y direction, because the x and y vibrations are not fully uncoupled. The rail, which is made of two blocks bolted together, is represented in Fig. 2. The lower block (200-mm wide and 50-mm thick) provides stiffness to the rail. Its length, $2L = 1.4$ m, is slightly larger than twice the inter-grating distance $L_{12} = 0.605$ m. The gratings, i.e. the mirrors of the laser standing waves, are fixed to the upper block, which has been almost completely cut in its middle to support the central grating. As a consequence, its

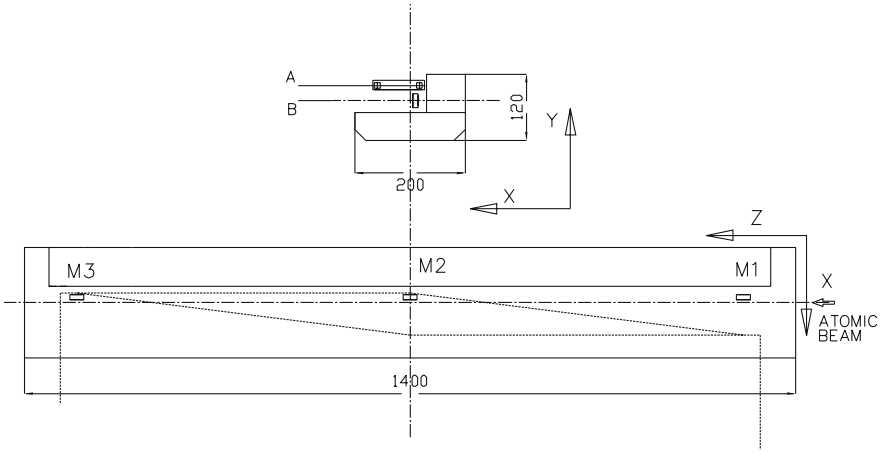

FIGURE 2 Drawings of our interferometer rail showing its shape and dimensions. *Upper drawing*: cross section of the rail showing the two blocks and their dimensions ($200 \times 50\,\mathrm{mm}^2$ for the *lower block*, $70 \times 70\,\mathrm{mm}^2$ for the *upper block*). The planes of the two interferometers are indicated (A for the atom interferometer, B for the optical interferometer). *Lower drawing*: top view of the rail, with some details: positions of the mirrors M_j for the three laser standing waves, positions of the atomic beam and of the laser beams of the Mach–Zehnder optical interferometer

contribution to the rigidity of the rail is probably very small and it will be neglected in the following calculation of the first bending resonance frequency $\omega_0/(2\pi)$: we use (15), with the full area $A \approx 1.49 \times 10^{-2}\,\mathrm{m}^2$, but, for the moment I_y, we consider only the lower-block contribution ($I_y \approx 3.3 \times 10^{-5}\,\mathrm{m}^4$). With $E = 72.4 \times 10^9\,\mathrm{N/m}^2$ and $\varrho = 2.79 \times 10^3\,\mathrm{kg/m}^3$, we calculate $\omega_0/2\pi \approx 437$ Hz.

When we built the suspension of the rail, the present analysis was not available and we made a very simple suspension: the rail is supported by three screws, two at one end and one at the other end, so that it can be finely aligned. Each screw is supported on a rubber block, model SC01 from Paulstra [21]. These rubber blocks, made to support machine tools, are ring shaped with a vertical axis. The technical data sheet gives only a rough estimate of the force constant K in the transverse direction, $K \approx 10^6\,\mathrm{N/m}$. As the total mass of our rail $\varrho AL \approx 58$ kg, the pendular oscillations are expected to be at $\omega_{\mathrm{osc}}/(2\pi) \approx 20$ Hz and $\omega_{\mathrm{rot}}/(2\pi) \approx 35$ Hz. We have not taken into account the mixing of these resonances due to $K_- \neq K_+$, considering that the dominant uncertainty comes from the spring-constant values.

4.3 *Test of the vibrations by optical interferometry*

Following the works of the research groups of Zeilinger [22, 23], Pritchard [17, 19] and Siu Au Lee [24, 25], the grating positions x_i are conveniently measured by a three-grating Mach–Zehnder optical interferometer. The phase $\Phi_{\mathrm{p,opt}}$ of the signal of such an optical interferometer is also given by (4), with a negligible time delay T:

$$\Phi_{\mathrm{p,opt}} = pk_{\mathrm{g,opt}}\delta(t)\,. \tag{19}$$

We have built such an optical interferometer [26]. The gratings from Paton Hawksley [27], with 200 lines/mm ($k_{\mathrm{g,opt}} = 1.26 \times 10^6\,\mathrm{m}^{-1}$), are used in the first diffraction order with a helium–neon laser at a 633-nm wavelength. The excitation of the rail by the environment gives very small signals, from which we deduce an upper limit of $\sqrt{\langle\delta(t)^2\rangle} < 3$ nm. This result is close to the noise (laser power noise and electronic noise) of the signal and the noise spectrum has not revealed any interesting feature.

Hence, we have made a spectroscopy of the rail vibrations in the frequency domain by exciting its vibrations by a small loudspeaker fixed on the rail, close to its center, with the coil moving in the x direction, so as to excite the x bending of the rail. The loudspeaker was excited by a sine wave of constant amplitude and we have recorded with a phase-sensitive detection the modulation of the optical interferometer signal. Figure 3 presents the detected signal in the region of the first intense resonance centered at $\omega_0/(2\pi) = 460.4$ Hz, with a rather large Q-factor, $Q \approx 60$. We have also observed a second resonance at $\omega_1/(2\pi) = 1375$ Hz, with $Q \approx 65$, with a 30 times weaker signal for the same voltage applied to the loudspeaker (the $n = 1$ resonance appears on the a amplitude and its detection by an optical interferometer, sensitive only to the b amplitude, is due to small asymmetries). The first resonance frequency 460.4 Hz is close to our estimate 437 Hz and the observed frequency ratio $\omega_1/\omega_0 \approx 2.99$ is also rather close to its theoretical value 2.76, so that we can assign these two

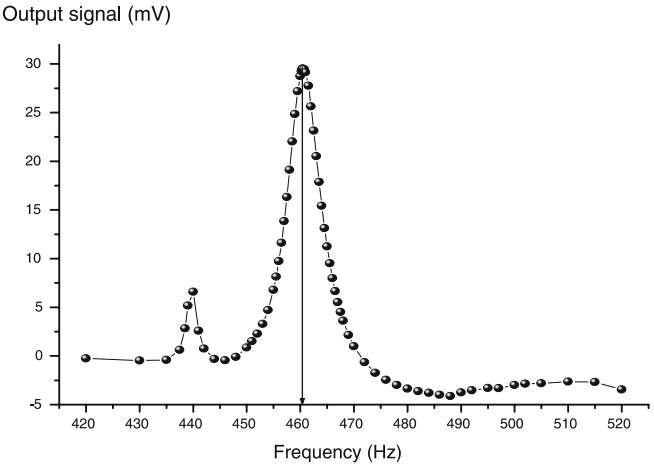

FIGURE 3 Response of the optical interferometer to an excitation of the rail oscillation: the modulation of the signal of the optical interferometer is plotted as a function of the frequency of the sine wave sent to the loudspeaker. We assign the main peak at 460.4 Hz as due to the first bending resonance but the weaker peak near 440 Hz is not assigned

resonances as the $n = 0$ and $n = 1$ bending resonances of the rail, the discrepancies being due to oversimplifications of our model.

We have not observed any clear signature of the pendular oscillations on the optical interferometer signal, probably because the excitation and detection efficiencies are very low. The detection of these pendular oscillations will be done in a future experiment, using seismometers.

4.4 *Seismic noise spectrum: measurement and consequences for the atom interferometer phase noise*

In a first step, we calculate the a and b amplitudes as a function of one noise amplitude $x_\pm(\omega)$, the other one being taken equal to 0. In all the calculations, we have used the simplifications $K_- = K_+ = K$ and $\mu_- = \mu_+ = \mu$. Figure 4 plots the ratios $|a(\omega)/x_\varepsilon(\omega)|^2$ and $|b(\omega)/x_\varepsilon(\omega)|^2$ as a function of the frequency $\nu = \omega/(2\pi)$: three resonances appear in the 1–10^3 Hz range and, as expected, a and b de-

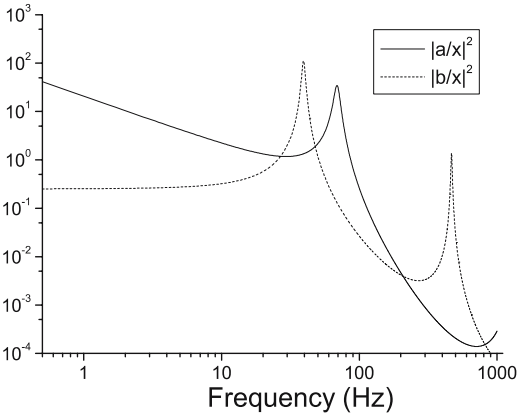

FIGURE 4 Logarithmic plot of the ratios $|a(\omega)/x_\varepsilon(\omega)|^2$ and $|b(\omega)/x_\varepsilon(\omega)|^2$ as a function of the frequency $\nu = \omega/(2\pi)$. Three resonances appear, which are the pendular oscillations, near 40 and 69 Hz, and the first bending resonance near 460 Hz

crease rapidly when $\omega > \omega_{\rm osc}, \omega_{\rm rot}$, a decrease interrupted for b by the first bending resonance at ω_0. In this calculation, we have not used the estimated parameters ($\omega_{\rm osc}/(2\pi) \approx 20$ Hz, $Q_{\rm osc} \approx 13$) of the first pendular resonance because, with the seismic noise spectrum described below, the predicted rms value of the bending amplitude is $\sqrt{\langle\delta(t)^2\rangle} \approx 15$ nm, considerably larger than measured. We have used larger values of $\omega_{\rm osc}/(2\pi) = 40$ Hz and $Q_{\rm osc} = 16$, so that the predicted rms value of the bending amplitude is reduced to $\sqrt{\langle\delta(t)^2\rangle} \approx 7$ nm. This value is still larger than what we measured, but we do not think that a more accurate tuning is reasonable without a direct measurement of the resonance frequency and Q-factors of the pendular resonances. In all the calculations, the first bending resonance frequency has been fixed to its measured value ω_0, $\omega_0/(2\pi) = 460.4$ Hz.

The seismic noise spectrum was recorded on our setup well before the operation of our interferometer. This spectrum presents several peaks appearing in the 8–60 Hz range and most of these peaks do not appear on a spectrum taken on the floor, because they are due to resonances of the structure supporting the vacuum pipes. As the peak frequencies have probably changed because of modifications of the experiment since the recording, we have replaced the recorded curve by a smooth curve just larger than the measured spectrum. This noise spectrum $|x_\varepsilon(\nu)|^2$ is plotted in Fig. 5. We have also extended the $\nu = 0.5$–100 Hz frequency range to $\nu = 0.5$–10^3 Hz, assuming the noise to be constant when 10^2 Hz $< \nu < 10^3$ Hz.

Figure 5 also plots the calculated phase noise spectrum $|\Phi_{\rm p}(\nu)/p|^2$, using (16) and the Sagnac phase noise spectrum $|\Phi_{\rm Sagnac}(\nu)/p|^2$ deduced from (16) by keeping only the term proportional to the a amplitude: clearly, the Sagnac phase noise is dominant except near the in-phase pendular oscillation and the first bending resonance. The bending resonance is in a region where the excitation amplitude is very low and, even after amplification by the resonance Q-factor, the contribution of the bending resonance to the total phase noise is fully negligible. In this calculation, we have assumed that the two excitation terms $x_\varepsilon(\nu)$ have the same spectrum but no phase relation, so that the cross-term $|x_+(\nu)x_-(\nu)|$ can be neglected. This last assumption is bad for very low frequencies, for which we expect $x_+(\nu) \approx x_-(\nu)$ (as the associated correction cancels the Sagnac term, we have not extended the $|\Phi_{\rm p}(\nu)/p|^2$ curves below 2 Hz), but the assumption is good as soon as the frequency is larger than the lowest frequency of a resonance of the structure supporting the vacuum chambers (near 8 Hz).

By integrating the phase noise over the frequency from 2 to 10^3 Hz, we obtain an estimate of the quadratic mean of the phase noise:

$$\langle\Phi^2\rangle = 0.16 p^2 \text{ rad}^2 . \tag{20}$$

This result is largely due to the Sagnac phase noise: the same integration carried only on the Sagnac phase noise gives $\langle\Phi^2_{\rm Sagnac}\rangle = 0.13 p^2$ rad^2. We are going to test this calculation, using the measurements of fringe visibility as a function of the diffraction order p.

4.5 *Fringe visibility as a test of phase noise in atom interferometers*

A phase noise $\Phi_{\rm p}$ induces a strong reduction of the fringe visibility $\mathcal{V}$:

$$\mathcal{V} = \mathcal{V}_{\max} \exp\left[-\langle\Phi_{\rm p}^2\rangle/2\right] , \tag{21}$$

assuming a Gaussian distribution of $\Phi_{\rm p}$. When the phase noise is due to inertial effects (see (3)), $\Phi_{\rm p}$ is proportional to the diffraction order p, $\Phi_{\rm p} = p\Phi_1$. The fringe visibility $\mathcal{V}$ is a Gaussian function of the diffraction order p [29]:

$$\mathcal{V} = \mathcal{V}_{\max} \exp\left[-\langle\Phi_1^2\rangle p^2/2\right] . \tag{22}$$

The atom interferometer of Siu Au Lee and co-workers [24, 25] and our interferometer [30] have been operated with the first three diffraction orders. The measured fringe visibility is plotted as a function of the diffraction order in Fig. 6 and Gaussian fits, following (22), represent very well the data. The

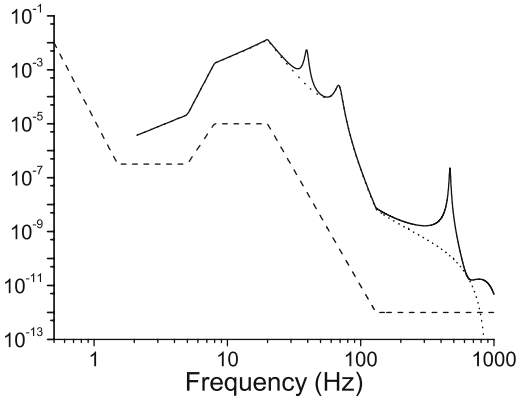

FIGURE 5 Calculated phase noise spectra $|\Phi(\nu)/p|^2$ (*full curve*) and $|\Phi_{\rm Sagnac}(\nu)/p|^2$ (*dotted curve*), both in rad^2/Hz, as a function of the frequency ν in Hz. The smoothed seismic noise spectrum $|x_\varepsilon(\nu)|^2$ in m^2/Hz used in the calculation is plotted (*dashed curve*) after multiplication by 10^{10}

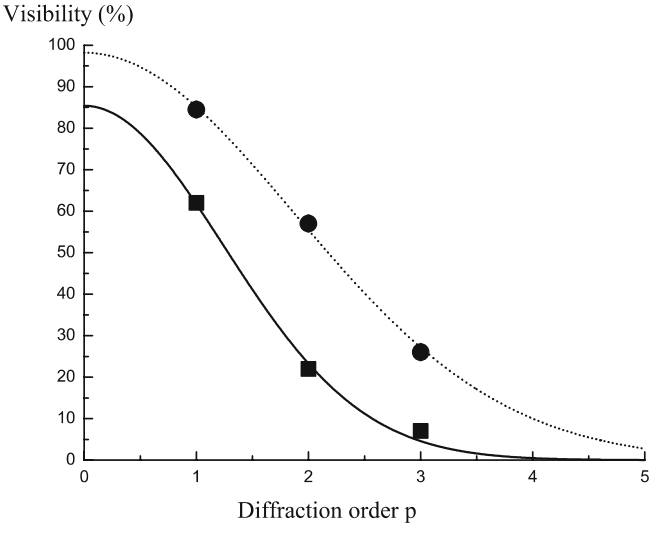

FIGURE 6 Fringe visibility as a function of the diffraction order p. Our measurements (*round dots*) are fitted by (22) with $\mathcal{V}_{\max} = 98 \pm 1\%$ and $\langle\Phi_1^2\rangle = 0.286 \pm 0.008$. The data points of Giltner and Siu Au Lee (*squares*) are also fitted by (22) with $\mathcal{V}_{\max} = 85 \pm 2\%$ and $\langle\Phi_1^2\rangle = 0.650 \pm 0.074$

quality of these fits suggests that phase noise of inertial origin is dominant and moreover that excellent visibility would be achieved in the absence of phase noise. With our data points, we deduce $\langle \Phi_p^2 \rangle = (0.286 \pm 0.008)\, p^2$. Our estimate given by (20) is 56% of this value and, considering the large uncertainty in several parameters (seismic noise, frequency and Q-factors of the pendular resonances), the agreement can be considered as good, the more so as other sources of phase noise may be present in our experiment.

5 How to further reduce the vibration phase noise in three-grating Mach–Zehnder atom interferometers

The phase noise induced by vibrations is very important and its reduction will considerably improve the operation of atom interferometers.

5.1 *Servo loops on the grating positions*

Pritchard and co-workers [17, 19] as well as Giltner and Siu Au Lee [24] have used servo loops to reduce the vibrational motion of the grating. The error signal was given by the optical Mach–Zehnder interferometer, which measures the instantaneous bending $\delta(t) = 2x_2(t) - x_1(t) - x_3(t)$ and, as recalled above, in both experiments, the error signal before correction was large. In the experiment of Pritchard and co-workers, the correction was applied to the second grating. In the limit of a perfect correction, the bending term in (4) is cancelled and this correction does not modify the Sagnac and the acceleration terms. The fact that acting on the second grating has no inertial effects is a somewhat surprising result, which can be explained by the symmetry of the Mach–Zehnder interferometer. In the experiment of Giltner and Siu Au Lee, the correction, which was applied to the third grating, cancels $\delta(t)$ but the Sagnac and acceleration terms are enhanced. In any case, the servo loop can reduce the instantaneous bending $\delta(t)$ but it cannot reduce the Sagnac and acceleration terms. We think that a very stiff rail is a better solution for Earth-based interferometers. For space-based experiments, the phase noise spectra due to vibrations are different and the above solution may not be optimum, because of the large weight of the rail.

5.2 *Possible improvements of the rail*

The stiffness of our rail has reduced to a low level the bending and acceleration terms in the phase noise of our interferometer. In our model, the rail stiffness is measured by only one parameter, the period T_0 of the lowest bending resonance, which scales with the rail length L like L^2. Our T_0 value, $T_0 = 2.2 \times 10^{-3}$ s, is still 3.8 times larger than the time of flight $T \approx 5.7 \times 10^{-4}$ s in our experiment (lithium beam mean velocity $u = 1065$ m/s, inter-grating distance $L_{12} = 0.605$ m) and the bending term in (18) is three times larger than the acceleration term. We can further reduce the bending term by reducing T_0, either by using an I-shaped rail to increase the I_y/A ratio or by using a material with a larger E/ϱ ratio than aluminium alloy (for example, silicon carbide).

A defect of our rail is that it has no symmetry axis and the x- and y-bending modes are partially mixed. As the moment I_x is considerably smaller than I_y, the bending resonances in the y direction are at lower frequencies than in the x direction. A better rail design should decouple almost completely the x- and y-vibrations.

5.3 *Possible improvements of the support and the rail suspension*

The structure supporting our interferometer is made of heavy steel rails, so that it is rather stiff with numerous resonances in the 8–60 Hz range. This structure and the vacuum pipes could be modelled by structural dynamics computational techniques and their vibration resonances could thus be predicted and optimized, but this is a very complex task.

The suspension of our rail is very primitive, with rather large spring constants and pendular resonances in the 20–100 Hz range. A very different choice was made by Toennies and co-workers [28]: the rail was suspended by wires, the restoring forces being due to gravity. The in-phase pendular oscillation frequency is $\omega_{osc} = \sqrt{g/l}$, where l is the wire length. For a typical l value, $l = 10$ cm, $\omega_{osc}/(2\pi) \approx 1.5$ Hz. In this experiment, a servo loop was necessary to reduce the amplitudes of the pendular motions.

Considering the seismic noise spectrum of Fig. 5, it seems clear that the resonances of the suspension should not be in the 5–30 Hz range, where there is an excess noise. Our choice is not ideal and the choice of Toennies and co-workers [28] seems better, as the seismic noise in this frequency range can be largely reduced. Very low pendular resonance frequencies, of the order of 0.1 Hz, can be achieved by clever designs (crossed-wire pendulum, Roberts linkage) and a large know-how has been developed for the construction of gravitational wave detectors LIGO, VIRGO, GEO, TAMA, etc. Without aiming at a comparable level of performance, it should be possible to build a very efficient suspension.

5.4 *Fringe visibility in atom interferometers*

Since the first atom interferometry experiments in 1991, many different interferometers have been operated and much effort has been made to improve these experiments. We are going to review the achieved fringe visibility, as this quantity is very sensitive to phase noise and to all phase-averaging effects (wavefront distortions, M-dependent phase due to magnetic field gradient, etc). We have considered only Mach–Zehnder atom interferometers in which the atom paths are substantially different, excluding for instance atomic clocks. Our review is not complete, in particular because some publications do not give the fringe visibility. The measured values of the visibility are plotted in Fig. 7. Some low values are not only due to phase noise but also to other reasons: maximum visibility less than 100% in the case of Moiré detection [17], parameters chosen to optimize the phase sensitivity [12]. Over a 15-year period, impressive progress has been achieved and, hopefully, the same trend will continue in the future. The comparison with optical interferometry is encouraging as very high fringe visibility is routinely achieved in this domain.

6 Conclusion

The present paper has analyzed the phase noise induced in a Mach–Zehnder atom interferometer by mechanical

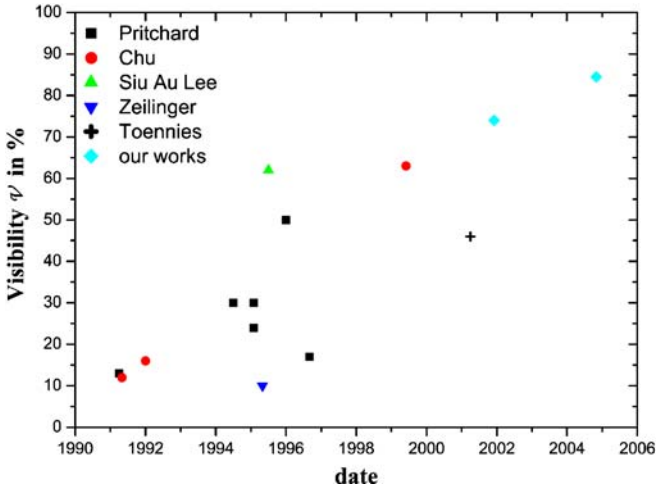

FIGURE 7 Fringe visibility $\mathcal{V}$ in Mach–Zehnder atom interferometers as a function of the date of submission of the publication. The data points are taken from the following publications: Pritchard's group [12, 17, 19, 31–34]; Chu's group [3, 4, 6]; Siu Au Lee's group [24, 25]; Zeilinger's group [23]; Toennies's group [35]; our works [30, 36]

vibrations. We have first recalled the inertial sensitivity of atom interferometers, following the presentation of Schmiedmayer et al. [19]. We have developed a simple but quite general one-dimensional model of the rail supporting the diffraction gratings. This model gives a unified description of the low-frequency dynamics, in which the rail behaves as a solid object, and the high- frequency domain, in which rail bending cannot be neglected.

We have then described the rail of our interferometer. Our design has produced a very stiff rail and the bending of the rail due to vibrations appears to be almost negligible, while it was important in several previous experiments. In the low-frequency range, up to the frequency of the rotational resonance of the rail suspension, the out-of-phase vibrations of the two ends of the rail induce rotations of the rail, which are converted into phase noise by the Sagnac effect: this is the dominant cause of inertial phase noise in our interferometer. A rapid decrease of the fringe visibility with the diffraction order has been observed by Siu Au Lee and co-workers [24, 25] and by our group [30]: the observed behavior is well explained as due to an inertial phase noise and the deduced phase noise value is in good agreement with a value deduced from our model of the rail dynamics, using as an input the seismic noise previously measured in our setup.

In the final section, we have presented a general discussion of the vibration-induced phase noise in three-grating Mach–Zehnder interferometers. A reduction of this noise is absolutely necessary in order to operate atom interferometers either with higher diffraction orders or with slower atoms. In our experiment, a large reduction of this noise should be obtained by improving the suspension of the interferometer rail. Finally, we have reviewed the published values of the fringe visibility obtained with atom interferometers, thus illustrating the rapid progress since 1991.

ACKNOWLEDGEMENTS We have received the support of CNRS MIPPU, of ANR and of Région Midi Pyrénées through a PACA-MIP network. We thank A. Souriau and J.-M. Fels for measuring the seismic noise in our laboratory.

Appendix: Amplitudes of vibration of the rail and Q-factors of its resonances

Equations (6) and (8) relate the values of the a, b, c and d amplitudes to $x_\varepsilon(\omega)$. Using (11), we eliminate c and d to obtain the system of equations (12), with

$$\begin{aligned}\alpha_\varepsilon &= [\cosh(\kappa L)\sin(\kappa L) - \sinh(\kappa L)\cos(\kappa L)]\cosh(\kappa L)\\ &\quad - 2(\kappa L)\cosh(\kappa L)\sinh(\kappa L)\sin(\kappa L)R_\varepsilon^{-1}\,,\\ \beta_\varepsilon &= [\cosh(\kappa L)\sin(\kappa L) + \sinh(\kappa L)\cos(\kappa L)]\sinh(\kappa L)\\ &\quad - 2(\kappa L)\cosh(\kappa L)\sinh(\kappa L)\cos(\kappa L)R_\varepsilon^{-1}\,,\\ \gamma_\varepsilon &= -(\kappa L)\cosh(\kappa L)\sinh(\kappa L)R_\varepsilon^{-1}\,, \end{aligned} \tag{A.1}$$

with $R_\varepsilon = \varrho AL\omega^2/(K_\varepsilon - \mathrm{i}\mu_\varepsilon\omega)$. From now on, $K_- = K_+ = K$ and $\mu_- = \mu_+ = \mu$. Then α, β and γ are independent of ε. R can be expressed as a function of $\omega_{\mathrm{osc}} = \sqrt{K/(\varrho AL)}$ and $Q_{\mathrm{osc}} = \varrho AL\omega_{\mathrm{osc}}/\mu$:

$$R = \omega^2 \Big/ \left[\omega_{\mathrm{osc}}^2 - \mathrm{i}\frac{\omega_{\mathrm{osc}}\omega}{Q_{\mathrm{osc}}}\right]. \tag{A.2}$$

We obtain a and b:

$$\begin{aligned} a &= \gamma(x_+ - x_-)/(2\alpha)\,,\\ b &= \gamma(x_+ + x_-)/(2\beta)\,. \end{aligned} \tag{A.3}$$

When $\kappa L \ll 1$, by expanding α, β and γ in powers of κL (up to the third order for α), we obtain

$$a = \frac{x_+ - x_-}{4\kappa L} \times \frac{3}{3-R}\,, \tag{A.4}$$

$$b = \frac{x_+ + x_-}{4(1-R)}\,. \tag{A.5}$$

b exhibits a resonance when $R = 1$ ($\omega = \omega_{\mathrm{osc}}$) and a when $R = 3$ ($\omega = \omega_{\mathrm{osc}}\sqrt{3}$). We have calculated the resonance Q-factors, in the weak-damping limit. For an isolated resonance, the Q-factor is related by $Q = 2\pi E_{\mathrm{tot}}/\Delta E$ to the total energy E_{tot} and the energy ΔE lost during one vibration period. We obtain

$$Q_{\mathrm{osc}} = \varrho AL\omega_{\mathrm{osc}}/\mu\,, \tag{A.6}$$

$$Q_{\mathrm{rot}} = \varrho AL\omega_{\mathrm{rot}}/(3\mu)\,, \tag{A.7}$$

$$Q_n = \varrho AL\omega_n g\kappa_n L/(8\mu)\,, \tag{A.8}$$

where the function $g(\kappa_n L)$ depends on the parity of n:

$$\begin{aligned} g(\kappa_n L) &= \left[1 + \frac{\sin(2\kappa_n L)}{2\kappa_n L}\right]\left[\frac{1}{\cos^2(\kappa_n L)} + \frac{1}{\cosh^2(\kappa_n L)}\right]\\ &\quad \text{for even } n\,,\\ &= \left[1 - \frac{\sin(2\kappa_n L)}{2\kappa_n L}\right]\left[\frac{1}{\sin^2(\kappa_n L)} + \frac{1}{\sinh^2(\kappa_n L)}\right]\\ &\quad \text{for odd } n\,. \end{aligned} \tag{A.9}$$

From the measured Q-factor of the first bending resonance ($n = 0$), we find $\mu \approx 560\,\mathrm{kg\,s^{-1}}$.

REFERENCES

1 J. Anandan, Phys. Rev. D **15**, 1448 (1977)
2 J.F. Clauser, Physica B **151**, 262 (1988)
3 M. Kasevich, S. Chu, Phys. Rev. Lett. **67**, 181 (1991)
4 M. Kasevich, S. Chu, Appl. Phys. B **54**, 321 (1992)
5 S.B. Cahn, A. Kumarakrishnan, U. Shim, T. Sleator, P.R. Berman, B. Dubetsky, Phys. Rev. Lett. **79**, 784 (1997)
6 A. Peters, K.Y. Chung, S. Chu, Nature **400**, 849 (1999)
7 A. Peters, K.Y. Chung, S. Chu, Metrologia **38**, 25 (2001)
8 M.J. Snadden, J.M. McGuirk, P. Bouyer, K.G. Haritos, M.A. Kasevich, Phys. Rev. Lett. **81**, 971 (1998)
9 J.M. McGuirk, G.T. Foster, J.B. Fixler, M.J. Snadden, M.A. Kasevich, Phys. Rev. A **65**, 033 608 (2002)
10 G.M. Tino, Nucl. Phys. B **113**, 289 (2002)
11 F. Riehle, T. Kisters, A. Witte, J. Helmcke, C.J. Bordé, Phys. Rev. Lett. **67**, 177 (1991)
12 A. Lenef, T.D. Hammond, E.T. Smith, M.S. Chapman, R.A. Rubenstein, D.E. Pritchard, Phys. Rev. Lett. **78**, 760 (1997)
13 T.L. Gustavson, P. Bouyer, M.A. Kasevich, Phys. Rev. Lett. **78**, 2046 (1997)
14 T.L. Gustavson, A. Landragin, M.A. Kasevich, Class. Quantum Grav. **17**, 2385 (2000)
15 F. Leduc, D. Holleville, J. Fils, A. Clairon, N. Dimarcq, A. Landragin, P. Bouyer, C.J. Bordé, in *Proc. 16th ICOLS*, ed. by P. Hannaford, A. Sidorov, H. Bachor, K. Baldwin (World Scientific, Singapore, 2004), pp. 68–70
16 A. Landragin, A. Clairon, N. Dimarcq, P. Teyssandier, C. Salomon, E.M. Rasel, W. Ertmer, Ch.J. Bordé, P. Tourrenc, P. Bouyer, M. Caldwell, R. Bingham, B. Kent, M. Sandford, P. Wolf, S. Airey, G. Bagnasco, in *Proc. ICATPP-7*, ed. by M. Barone, E. Borchi, J. Huston, C. Leroy, P.G. Rancoita, P. Riboni, R. Ruchti (World Scientific, Singapore, 2002), pp. 16–22
17 D.W. Keith, C.R. Ekstrom, Q.A. Turchette, D.E. Pritchard, Phys. Rev. Lett. **66**, 2693 (1991)
18 A. Stibor, K. Hornberger, L. Hackermüller, A. Zeilinger, M. Arndt, Laser Phys. **15**, 10 (2005)
19 J. Schmiedmayer, M.S. Chapman, C.R. Ekstrom, T.D. Hammond, D.A. Kokorowski, A. Lenef, R.A. Rubinstein, E.T. Smith, D.E. Pritchard, in *Atom Interferometry*, ed. by P.R. Berman (Academic, San Diego, 1997), p. 1
20 L. Landau, E. Lifchitz, *Theory of Elasticity* (Pergamon, Oxford, 1986)
21 Paulstra company, web site http://www.paulstra-vibrachoc.com
22 M. Gruber, K. Eder, A. Zeilinger, Phys. Lett. A **140**, 363 (1989)
23 E.M. Rasel, M.K. Oberthaler, H. Batelaan, J. Schmiedmayer, A. Zeilinger, Phys. Rev. Lett. **75**, 2633 (1995)
24 D.M. Giltner, R.W. McGowan, Siu Au Lee, Phys. Rev. Lett. **75**, 2638 (1995)
25 D.M. Giltner, Ph.D. thesis, Colorado State University, Fort Collins (1996)
26 A. Miffre, R. Delhuille, B. Viaris de Lesegno, M. Büchner, C. Rizzo, J. Vigué, Eur. J. Phys. **23**, 623 (2002)
27 Paton Hawksley Education Ltd., UK, web site http://www.patonhawksley.co.uk/
28 J.P. Toennies, private communication (2003)
29 R. Delhuille, A. Miffre, B. Viaris de Lesegno, M. Büchner, C. Rizzo, G. Trénec, J. Vigué, Acta Phys. Pol. **33**, 2157 (2002)
30 A. Miffre, M. Jacquey, M. Büchner, G. Trénec, J. Vigué, Eur. Phys. J. D **33**, 99 (2005)
31 C.R. Ekstrom, J. Schmiedmayer, M.S. Chapman, T.D. Hammond, D.E. Pritchard, Phys. Rev. A **51**, 3883 (1995)
32 J. Schmiedmayer, M.S. Chapman, C.R. Ekstrom, T.D. Hammond, S. Wehinger, D.E. Pritchard, Phys. Rev. Lett. **74**, 1043 (1995)
33 T.D. Roberts, A.D. Cronin, D.A. Kokorowski, D.E. Pritchard, Phys. Rev. Lett. **89**, 200 406 (2002)
34 M.S. Chapman, C.R. Ekstrom, T.D. Hammond, R.A. Rubenstein, J. Schmiedmayer, S. Wehinger, D.E. Pritchard, Phys. Rev. Lett. **74**, 4783 (1995)
35 Work of J.P. Toennies, R. Brühl, quoted in D. Meschede, *Gerthsen Physik*, 22nd edn. (Springer, Berlin Heidelberg, 2003), p. 709
36 R. Delhuille, C. Champenois, M. Büchner, L. Jozefowski, C. Rizzo, G. Trénec, J. Vigué, Appl. Phys. B **74**, 489 (2002)